A THEORETICAL STUDY ON THE SUCROSE GAP TECHNIQUE AS APPLIED TO MULTICELLULAR MUSCLE PREPARATIONS

I. SALINE-SUCROSE INTERDIFFUSION

E. LAMMEL, *Department of Physiology, Philipps Universität Marburg, D-3550 Marburg/Lahn, Federal Republic of Germany*

ABSTRACT Voltage-clamp analysis of membrane currents in multicellular muscle preparations by means of the sucrose gap method is complicated by diffusion of saline and sucrose in the interstitial fluid spaces. This paper is the first part of a theoretical study made to analyze electrical events related to this diffusion process. Concentration profiles of ions and sucrose (both axial and radial) were computed by solving diffusion equations with boundary conditions appropriate for the different types of preparations and experimental arrangements used. In addition to steady-state solutions, analytical expressions were derived that describe the time-course with which concentration profiles become established after a stepwise change of the solute concentration in one of the compartments of the sucrose gap apparatus. The model accounts for the presence of an endothelial surface layer, or endocardium, which acts as an external diffusion barrier and is important in determining concentration gradients of solutes within heart cell preparations. Results of numerical computations dealing with several cases of experimental interest are presented.

INTRODUCTION

Much of the analysis of the electrical membrane currents in multicellular muscle preparations is based on methods using either a single or double sucrose gap apparatus (see Johnson and Lieberman, 1971; Morad and Goldman, 1973; Trautwein, 1973; Bülbring and Shuba, 1976; Beeler and McGuigan, 1978). There are many important results obtained with these methods; several sources of error associated with them have been discussed and experimentally tested (Johnson and Lieberman, 1971; Kootsey and Johnson, 1972; Tarr and Trank, 1971, 1974; Ramón et al., 1975; Poindessault et al., 1976; Attwell and Cohen, 1977; Beeler and McGuigan, 1978). However, one of the shortcomings of the method has not received the attention it deserves. This is related to the fact that there is no sharp transition between sucrose and adjacent electrolyte solution, except at the surface of the muscle fiber bundle. Inside the bundle diffusion of ions and sucrose takes place along the interstitial fluid spaces, resulting in complex concentration changes. The properties of the ion concentration profiles that are established are important in determining, among other things, (*a*) the driving forces of several membrane currents, (*b*) the size of the membrane resistance, (*c*) the shunt resistance of current recording, and (*d*) the position and size of the liquid junction potential set up by the diffusing ions of different mobilities. The aim of this and two subsequent papers was to explore both the nature and the extent of the complications that arise from these

factors. The present study deals with the diffusion processes occurring in different preparations and experimental arrangements. The accompanying paper will be concerned with the analysis of the cellular outward (potassium) currents, while in a third, both the outward and "activated" inward (sodium or calcium) currents will be considered.

DIFFERENTIAL EQUATIONS OF DIFFUSION AND BOUNDARY CONDITIONS

For the present mathematical treatment, the structure of a heart trabecula, or bundle, has been simplified as illustrated in Fig. 1 *C*: the bundle is taken to be (*a*) of cylindrical shape, (*b*) to contain fibers, all cylinders of equal diameter, distributed in a random fashion, and (*c*) to be surrounded by a thin homogeneous diffusion barrier, representing the endothelium cell sheath (or endocardium) which separates the external medium from the interstitial fluids surrounding the individual heart fibers. Thus, the model ignores the variation of fiber size and shape as well as the presence of narrow spaces and clefts between muscle cells (cf. Page and Niedergerke, 1972; Sommer and Johnson, 1979). It also does not take into account that diffusion (or permeation) through the endothelial cell sheath occurs in discrete regions, the gaps between adjacent cells (Page and Niedergerke, 1972). Further simplifications are (*a*) ion fluxes into and out of the cells are assumed to be small enough to modify the external diffusion process only to a negligibly small extent (see Approximations) (*b*) the diffusion coefficients of both electrolytes and nonelectrolytes (sucrose in the present case) are taken to be unaltered as the concentration of the solutes changes, and (*c*) cross effects between different solutes are neglected. (The diffusion of Na^+Cl^- or K^+Cl^-, for example, is treated as if only the particular salt were present in a range of low concentrations.)

We consider both radial and longitudinal diffusion of solute through the interstitial fluid spaces, looking first at a small volume element, an annulus situated concentrically with respect to the axis (z) of the bundle (surface radius r_0), of width Δr and length Δz. Radial

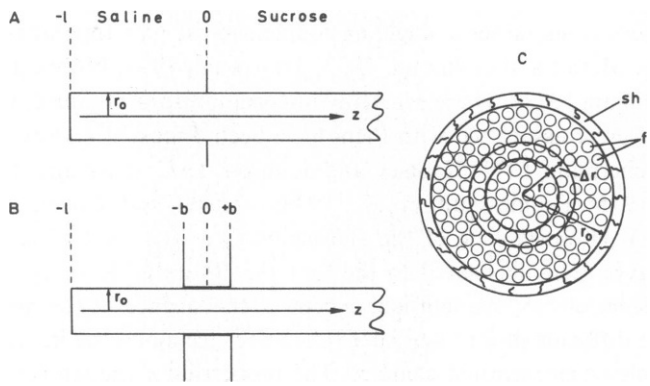

FIGURE 1 Geometrical model of heart cell bundle and its position across a saline-sucrose junction. *A*, no partition; *B*, partition of width $2b$ present between the two fluid compartments; *C*, cross section through bundle and its constituent fibers (f) surrounded by endothelium cell sheath (sh). The drawing is not to scale: endothelium cell sheath in most regions (except at point of cell nucleus) is much thinner than average fiber diameter.

diffusion flux M_r entering the annulus at r is given by the first law of diffusion as

$$M_r = -\frac{\alpha}{\beta} 2\pi r \Delta z D \frac{\partial c}{\partial r} \tag{1}$$

where c is the concentration of the diffusing solute, D is the diffusion coefficient, and α is the fractional circumference at radius r that is available for radial diffusion, i.e., not occupied by cells. β is a factor that accounts for the increased path length that solute particles must generally follow around the fibers instead of being able to pass through the space occupied by the fibers. On the other hand, the longitudinal flux M_z entering the annulus at z is

$$M_z = -\rho 2\pi r \Delta r D \frac{\partial c}{\partial z}, \tag{2}$$

where ρ is the area per cross section of bundle taken up by the interstitial fluid spaces. Fluxes entering and leaving the annulus must be equal to the rate with which the quantity of solute in the interstitial fluid spaces within the annulus changes:

$$M_r(r, z) - M_r(r + \Delta r, z) + M_z(r, z) - M_z(r, z + \Delta z) = \rho 2\pi r \Delta r \Delta z \frac{\partial c}{\partial t} \tag{3}$$

or

$$-\frac{\partial M_r}{\partial r} \Delta r - \frac{\partial M_z}{\partial z} \Delta z = \rho 2\pi r \Delta r \Delta z \frac{\partial c}{\partial t}. \tag{4}$$

After combination with Eqs. 1 and 2, Eq. 4 gives

$$D\left[k \frac{1}{r} \frac{\partial}{\partial r}\left(r \frac{\partial c}{\partial r}\right) + \frac{\partial^2 c}{\partial z^2}\right] = \frac{\partial c}{\partial t} \tag{5}$$

where

$$k = \frac{\alpha}{\beta \rho}. \tag{6}$$

At the bundle surface, just underneath the endothelial cell sheath, the flux entering the bundle must equal that which passes through the surface sheath:

$$-\rho k D \left(\frac{\partial c}{\partial r}\right)_{r=r_0} = P_m[c(r_0, z) - c_0] \tag{7}$$

where P_m is the permeability coefficient of the sheath and c_0 the concentration of solute in the external medium. The right-hand side of Eq. 7 corresponds to that of Eq. 2 used by Page and Niedergerke (1972) to describe the passage of solutes through the endothelium cell sheath. Eq. 7 serves to provide the basis of several boundary conditions used in solving Eq. 5. Before presenting these solutions, two additional points should be considered.

(*a*) In certain, well-defined experimental conditions, i.e., when using thin bundles whose surface layer is of low solute permeability, the rate-limiting step for solute movement into and out of the bundle is provided by permeation of the solute through the surface layer. A useful

approximation can be obtained for this case by neglecting radial diffusion in the interstitial fluid spaces altogether. The diffusion equation then simplifies to read

$$\frac{\partial c}{\partial t} = D\frac{\partial^2 c}{\partial z^2} - \frac{P_m}{\rho}\frac{A_s}{A_c}\left(c - c_0\right) \tag{8}$$

where the first term on the right-hand side relates to longitudinal diffusion and the second relates to surface permeation. A_s is the surface area per unit length and A_c the cross-sectional area of the bundle ($A_s/A_c = 2/r_0$ for the cylinder in Fig. 1 *C*).

(*b*) It is desirable to express the two geometrical constants α and β of Eq. 6 in terms of ρ, the volume fraction of interstitial fluid spaces. With regard to α, the proportion of bundle circumference (at various r) unoccupied by heart cells, it can be shown that the identity $\alpha = \rho$ holds to a good approximation (ρ being independent of r), provided that r_0 is large compared with the fiber radius. This is the case for all heart bundles considered in this and the subsequent papers. Intuitively, this result immediately follows from the assumption of a random cell distribution, but the mathematical proof is fairly lengthy and has therefore been omitted. β, the factor expressing the increased diffusion pathway, was calculated following the procedure of McLennan (1956):

$$\beta = 1 + \frac{4}{\pi}\left(1 - \rho\right)\left(1 - \frac{\pi}{4}\right). \tag{9}$$

Combining the expressions for α and β with Eq. 6 one obtains

$$k = \left[1 + \frac{4}{\pi}\left(1 - \rho\right)\left(1 - \frac{\pi}{4}\right)\right]^{-1}. \tag{10}$$

For a related approach to account for the effect of tortuosity see Adrian et al. (1969), Schneider (1970), and Mathias et al. (1977).

STEADY-STATE SOLUTIONS

The first and main part of this paper is concerned with the concentration profiles maintained within the extracellular fluid spaces of the muscle bundle by the steady diffusion flux of saline into the sucrose region, or of sucrose in the reverse direction. In a later section the time-course with which some of these profiles are established will also be considered. To start with, the equations solved deal with a single saline-sucrose junction. Solutions appropriate to the more complex situation of sucrose gap arrangements, where two or four such junctions are present, can be obtained by applying the superposition principle.

The basic differential equation used is derived from Eq. 5 and reads

$$k\frac{1}{r}\frac{\partial}{\partial r}\left(r\frac{\partial c}{\partial r}\right) + \frac{\partial^2 c}{\partial z^2} = 0. \tag{11}$$

Two boundary conditions common to many cases follow from the physical arrangement of the bundle (see Fig. 1): a segment, of length l, of the bundle is taken to protrude into the test compartment containing saline. (In order to keep potential changes along this segment small, this has to be kept short compared with the length of the electrical space constant; see Johnson and Lieberman, 1971). At the far end of this segment, where $z = -l$, the concentration

gradient across the endothelium cell sheath is taken to be zero, since at this point the sheath has been destroyed either by the ligature placed around the trabecula (New and Trautwein, 1972; Goldman and Morad, 1977) or by transverse sectioning of the trabecula, as some authors prefer (Reuter and Scholz, 1977). The trabecula section that extends into the sucrose compartment is taken to be of infinite length. If the concentration in the left-hand side compartment is maintained at c_0, that in the right-hand side at zero, one has

$$c(r, -l) = c_0. \tag{12a}$$

$$c(r, \infty) = 0. \tag{12b}$$

In sucrose gap experiments two types of chamber are used: in one (Fig. 1 *B*), saline and sucrose compartments are separated by rubber membranes or vaseline seals (Berger, 1963; Rougier et al., 1968; Brown and Noble, 1969; Beeler and Reuter, 1970; Morad and Orkand, 1971; New and Trautwein, 1972; McGuigan, 1974; de Hemptinne, 1976); in the other type (Fig. 1 *A*) such partitions are absent (Anderson, 1969; Haas et al., 1970; Tarr and Trank, 1971, 1974; Harrington and Johnson, 1973, de Hemptinne, 1976). This means that two sets of equations are required: the one appropriate for the absence of partitions or seals is more simple mathematically and is therefore treated first.

Partition Between Electrolyte and Sucrose Compartment Is Negligible

For this case the second set of boundary conditions derived from Eq. 7 is

$$-\rho k D\left(\frac{\partial c}{\partial r}\right)_{r=r_0} = P_m[c(r_0, z) - c_0], \quad z < 0 \tag{13a}$$

$$-\rho k D\left(\frac{\partial c}{\partial r}\right)_{r=r_0} = P_m c(r_0, z), \quad z > 0. \tag{13b}$$

The solution of Eqs. 11 satisfying Eqs. 12a, b and 13a, b as well as the continuity conditions for both c and $\partial c/\partial z$ (continuity of diffusion flux) at $z = 0$ was derived by standard methods given in Carslaw and Jaeger (1959, chapts. 7 and 8). The result obtained is

$$c = c_0\left[1 - 2\sum_{n=1}^{\infty} \frac{J_0(\beta_n r/r_0)}{\beta_n(1 + \beta_n^2/L^2)J_1(\beta_n)} \exp(-\beta_n l\sqrt{k}/r_0) \sinh(\beta_n(l + z)\sqrt{k}/r_0)\right], \; z \leq 0 \tag{14a}$$

$$c = 2c_0\sum_{n=1}^{\infty} \frac{J_0(\beta_n r/r_0)}{\beta_n(1 + \beta_n^2/L^2)J_1(\beta_n)} \cosh(\beta_n l\sqrt{k}/r_0) \exp(-\beta_n(l + z)\sqrt{k}/r_0), \; z \geq 0. \tag{14b}$$

β_n are the positive roots of

$$\beta J_1(\beta) - L J_0(\beta) = 0. \tag{15}$$

J_0 and J_1 are the Bessel functions of the first kind, and of order zero and one, respectively, where

$$L = \frac{P_m r_0}{\rho k D} \tag{16}$$

or after combination with Eq. 10

$$L = \frac{P_m r_0 \left[1 + \frac{4}{\pi}(1 - \rho)\left(1 - \frac{\pi}{4}\right)\right]}{\rho D}. \tag{17}$$

For many problems it is sufficient to know the average concentration $\bar{c}(z)$ in a cross section at any z. This is defined by

$$\bar{c}(z) = \frac{2}{r_0^2}\int_0^{r_0} rc(r, z)\, dr. \tag{18}$$

Integration of Eq. 18 after substituting for $c(r, z)$ Eqs. 14a and b gives

$$\bar{c} = c_0\left[1 - 4\sum_{n-1}^{\infty}\frac{1}{\beta_n^2(1 + \beta_n^2/L^2)}\exp(-\beta_n l\sqrt{k}/r_0)\sinh(\beta_n(z + l)\sqrt{k}/r_0)\right], z \le 0 \tag{19a}$$

$$\bar{c} = 4c_0\sum_{n-1}^{\infty}\frac{1}{\beta_n^2(1 + \beta_n^2/L^2)}\cosh(\beta_n l\sqrt{k}/r_0)\exp(-\beta_n(z + l)\sqrt{k}/r_0), z \ge 0. \tag{19b}$$

Concentration profiles of physiological interest calculated by means of Eqs. 19a, b are plotted in Figs. 6 and 7 and discussed in some detail in Conclusions. However, it is instructive here to illustrate the results of Eqs. 14 and 19 in a more general way, simplifying the geometrical situation by considering a bundle whose ends are both sufficiently far away from the saline-sucrose junction so that $-l \sim -\infty$ (Fig. 1 *A*). For this condition Eqs. 14a, b reduce to

$$c = c_0\left[1 - \sum_{n-1}^{\infty}\frac{J_0(\beta_n r/r_0)}{\beta_n(1 + \beta_n^2/L^2)J_1(\beta_n)}\exp(\beta_n z\sqrt{k}/r_0)\right], z \le 0 \tag{20a}$$

$$c = c_0\sum_{n-1}^{\infty}\frac{J_0(\beta_n r/r_0)}{\beta_n(1 + \beta_n^2/L^2)J_1(\beta_n)}\exp(-\beta_n\sqrt{k}/r_0), z \ge 0 \tag{20b}$$

and Eqs. 19a, b to

$$\bar{c} = c_0\left[1 - 2\sum_{n-1}^{\infty}\frac{1}{\beta_n^2(1 + \beta_n^2/L^2)}\exp(\beta_n z\sqrt{k}/r_0)\right], z \le 0 \tag{21a}$$

$$\bar{c} = 2c_0\sum_{n-1}^{\infty}\frac{1}{\beta_n^2(1 + \beta_n^2/L^2)}\exp(-\beta_n z\sqrt{k}/r_0), \quad z \ge 0. \tag{21b}$$

Concentrations, in units of c_0 and calculated with Eq. 20b, are plotted in Fig. 2 against the dimensionless parameter r/r_0, for various values of z, also transformed into a dimensionless variable, $zk^{1/2}/r_0$. (The series solutions converge fairly rapidly. The first six terms were computed to arrive at the curves shown in this and all other figures.) As is seen, concentration profiles so obtained are critically dependent on L (Eq. 16), which combines the important physical contraints of the diffusion process. Of the four values of L for which solutions are illustrated, probably only two, that for $L = 0.5$ and 1.5, are of interest when considering intact heart bundles for which the estimates of L extend from values between 0.3 and 1.5 (see Discussion). Noting, on inspection of Fig. 2, the extent of deviation of curves shown from horizontal straight lines it is clear (remembering the definition of L) that radial concentration

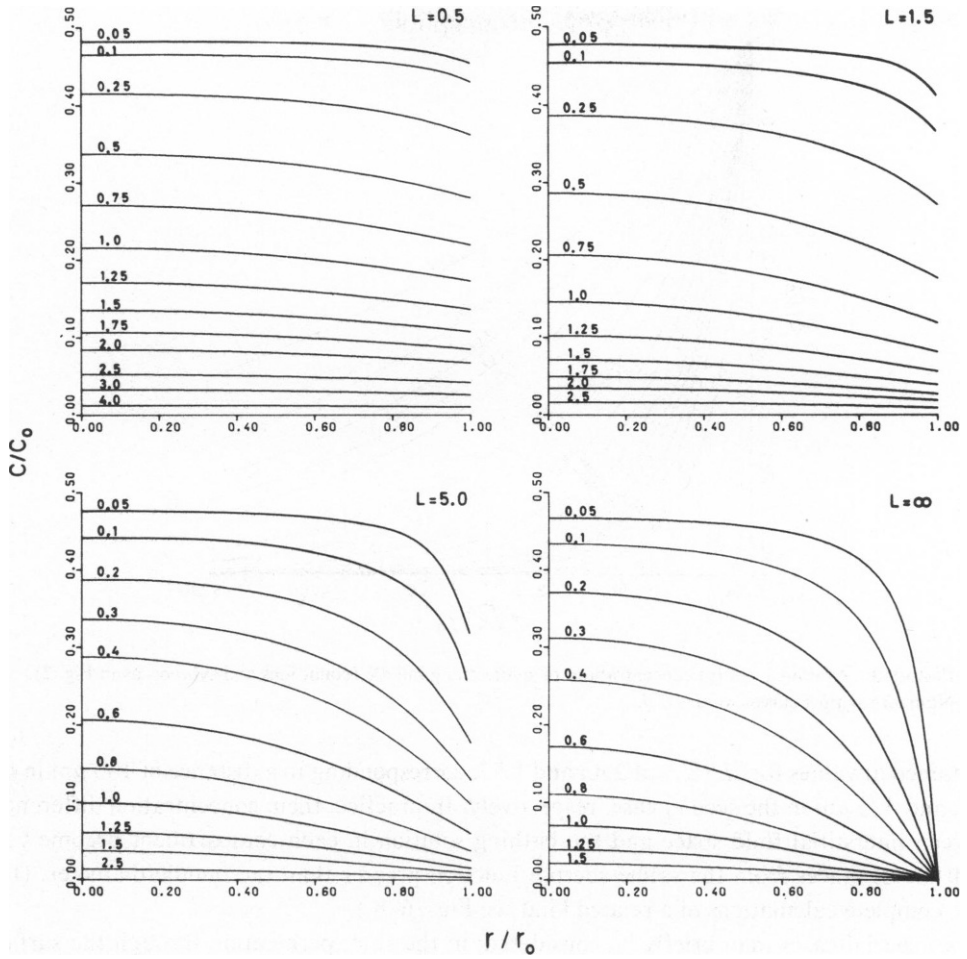

FIGURE 2 Steady concentration profiles of solute in interstitial fluid spaces of cylindrical muscle bundle (position as indicated in Fig. 1*A* with $-l \rightarrow -\infty$); external concentration of solute: c_0 for $z < 0$ and zero for $z > 0$. Plot of concentration c against radius r, both in dimensionless form (r_0 = surface radius of cylinder). Numbers against curves, values of $zk^{1/2}/r_0$, i.e. normalized distance along bundle; for definition of k and L see Eqs. 6 and 16. Concentrations for negative z, also in Fig. 3, can be obtained by means of the symmetry relation $c(-z)/c_0 = 1 - c(z)/c_0$ (see Eqs. 20a,b).

gradients within a bundle diminish as P_m and r_0 decline. P_m is, however, directly proportional to D (e.g. Page and Niedergerke, 1972) and both the parameter L and the steady-state distribution of solutes are therefore independent of the diffusion coefficient used (see Eq. 17 and note that the solution of Eq. 11 does not explicitly contain D). Fig. 3 illustrates the distribution of $\bar{c}$, along bundle length obtained with Eq. 21b, i.e., the decline of $\bar{c}$ from the level $c_0/2$ at $z = 0$ with increasing z. To provide a numerical example, we have calculated the distance from the sucrose-saline junction at which $\bar{c}$ has reached 10% of $\bar{c}$ at $z = 0$ (i.e., to 5% of the total concentration difference) for a bundle from frog atrium (100 μm Diam) and dog ventricle (500 μm Diam; Beeler and Reuter, 1970). Using the values $L = 0.5$ for the frog atrium and $L = 1.5$ for the dog ventricle and $k = 0.83$ for both (see Parameter Values), this level

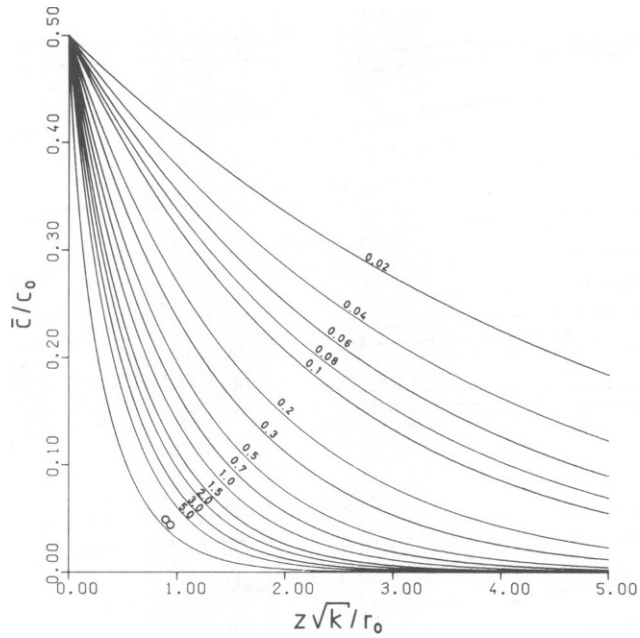

FIGURE 3 Average (steady) concentrations of solute along bundle (conditions and symbols as in Fig. 2). Numbers against curves, values of L.

is attained at values for $zk^{1/2}/r_0$ of 2.45 and 1.55, corresponding to a distance of 135 μm in the first, and 425 μm in the second case, respectively. In practice, then, concentration differences between interstitial fluid space and the bathing solution in each compartment become very small for distances from the saline-sucrose junction greater than the bundle diameter. (For more complete calculations of a related kind see Figs. 6–8.)

Two special cases may briefly be considered: in the first, permeation through the surface layer is quite rapid (i.e., P_m is large), a condition that would be applicable, for example, to a trabecula whose endocardium had been removed. In the second, the permeability coefficient is low and the bundle diameter small so that radial diffusion can be neglected to a first approximation.

TRABECULA WITHOUT SURFACE LAYER Equations that describe the concentration distribution under this condition can be derived as limits from those given before. Since $L \to \infty$ as $P_m \to \infty$ (see Eq. 16) the factor $J_0(\beta_n r/r_0)/[\beta_n(1 + \beta_n^2/L^2)\, J_1(\beta_n)]$ in Eqs. 14a, b and 20a, b has to be replaced by $J_0(\alpha_n r/r_0)/[\alpha_n J_1(\alpha_n)]$ where

$$\alpha_n = \lim_{L \to \infty} \beta_n \text{ and } J_0(\alpha_n) = 0.$$

(See Eq. 15). In Eqs. 19a, b and 21a, b the factor $[\beta_n^2(1 + \beta_n^2/L^2)]^{-1}$ simply becomes α_n^{-2}.

THIN BUNDLE WITH SURFACE LAYER OF LOW PERMEABILITY The equations appropriate to this case simplify (cf. Eq. 8) to become

$$\frac{d^2c}{dz^2} - \frac{1}{\Lambda^2}(c - c_0) = 0, \quad z < 0 \tag{22a}$$

$$\frac{d^2c}{dz^2} - \frac{1}{\Lambda^2}c = 0, \quad z > 0 \tag{22b}$$

where

$$\Lambda = \sqrt{\frac{\rho D A_c}{P_m A_s}}. \tag{22c}$$

The solution satisfying the boundary conditions (Eq. 12a, b) and the continuity conditions for c and dc/dz at $z = 0$ is

$$c = c_0\{1 - \exp(-\ell/\Lambda)\sinh[(z + \ell)/\Lambda]\}, \quad z \leq 0 \tag{23a}$$

$$c = c_0 \cosh(\ell/\Lambda)\exp[-(z + \ell)/\Lambda], \quad z \geq 0 \tag{23b}$$

and for $-l \rightarrow -\infty$:

$$c = c_0\left[1 - \frac{1}{2}\exp(z/\Lambda)\right], \quad z \leq 0 \tag{24a}$$

$$c = \frac{c_0}{2}\exp(-z/\Lambda), \quad z \geq 0. \tag{24b}$$

Λ is a space constant, analogous to the electrical space constant, λ, of single nerve or muscle cell. In this analogy P_m and D correspond to $(R_m)^{-1}$ and $(R_i)^{-1}$, i.e., the reciprocals of the specific membrane and intracellular resistance, respectively. It may also be noted that Λ is independent of D, a property that it shares with the parameter L.

Partition of Finite Width Separating Saline and Sucrose Compartments

A complete mathematical description of this situation (Fig. 1 *B*) requires the complex techniques of the so-called mixed boundary problem (Kantorovich and Krylov, 1958).

However, there are two cases in which solutions can be obtained by fairly simple means. The first is a bundle in which the endothelial cell sheath (or endocardium) is absent. This problem was recently treated by Attwell and Cohen (1977) and therefore needs not be discussed. The second concerns a bundle in which radial diffusion in the interstitial spaces can be neglected; this case was treated in Eqs. 22–24 for the situation of a saline-sucrose junction without partition. Assuming a partition of width $2b$ (extending from $-b \leq z \leq b$; Fig. 1 *B*) the appropriate differential equations become

$$\frac{d^2c}{dz^2} - \frac{1}{\Lambda^2}(c - c_0) = 0, \quad -\ell < Z < -b \tag{25a}$$

$$\frac{d^2c}{dz^2} = 0, \quad -b < z < b \tag{25b}$$

$$\frac{d^2c}{dz^2} - \frac{1}{\Lambda^2}c = 0, \quad z > b. \tag{25c}$$

As Beeler and McGuigan (1978) pointed out, rubber membranes used as partitions tend to compress the tissue bundle; as a result, the concentration profiles are altered. In deriving

equations that account for such compression effects it is convenient to define the cross-sectional area available for diffusion underneath the partition by $(\rho A_c)_p$ and that outside it by $(\rho A_c)_0$. Solutions of Eq. 25 are required which satisfy the continuity condition for $(\rho A_c \cdot dc/dz)$ at $z = -b$ and $z = +b$, with the continuity in c and the boundary conditions Eqs. 12a,b. These solutions are

$$c = c_0\left\{1 - \frac{\sinh[(\ell + z)/\Lambda]}{(2bH/\Lambda + 1)\cosh[(\ell - b)/\Lambda] + \sinh[(\ell - b)/\Lambda]}\right\}, \quad -\ell \le z \le -b \tag{26a}$$

$$c = c_0\frac{H(b - z)/\Lambda + 1}{1 + 2bH/\Lambda + \tanh[(\ell - b)/\Lambda]}, \quad -b \le z \le b \tag{26b}$$

$$c = c_0\frac{\exp[(b - z)/\Lambda]}{1 + 2bH/\Lambda + \tanh[(\ell - b)/\Lambda]}, \quad z \ge b \tag{26c}$$

where H is defined as

$$H = (\rho A_c)_0/(\rho A_c)_p. \tag{27}$$

Examples of practical interest were worked out using Eqs. 26 and 27 and are presented in connection with Fig. 7 in the Discussion.

KINETICS OF THE DIFFUSION PROCESS

We are seeking the time-course with which concentration profiles in muscle bundles build up or decline when the solute concentration in one of the fluid compartments is altered. For the sake of brevity, only one case will be treated, i.e., that of a trabecula extending a long way to both sides from a single saline-sucrose junction (for the steady-state solution of this case, see Figs. 2 and 3). We consider a trabecula, positioned as shown in Fig. 1 *A* (but $-l \rightarrow -\infty$), with the initial solute concentration $c = c_0$ in the one (left-hand) compartment and $c = 0$ in the other. At time zero the concentration in the left-hand compartment is suddenly changed from c_0 to c_1. The appropriate initial and boundary conditions for the differential Eq. 5 are

$$c(r, z, 0) = c_i(r, z) \tag{28a}$$

where $c_i(r,z)$ is the initial concentration at any point within the bundle given by Eq. 20 a,b,

$$c(r, -\infty, \infty) = c_1 \tag{28b}$$

$$c(r, +\infty, \infty) = 0 \tag{28c}$$

$$-\rho kD\left(\frac{\partial c}{\partial r}\right)_{r=r_0} = P_m[c(r_0, z, t) - c_1], \; z < 0 \tag{28d}$$

$$-\rho kD\left(\frac{\partial c}{\partial r}\right)_{r=r_0} = P_m c(r_0, z, t), \; z > 0. \tag{28e}$$

The solution was derived by following the procedure given by Carslaw and Jaeger (1959, p. 29) of solving, consecutively, two simpler problems. One is time independent and has already been treated (Eq. 20a,b); the other is dependent on time, t, as well as on the space variables r

and z. We take $c_f(r, z)$ to be the known solution of (time independent) Eq. 11 satisfying the conditions 12a,b (with $-1 \rightarrow -\infty$) and 13a,b, with c_0 replaced by c_1. We also define $c_t(r, z, t)$ as a function that satisfies Eq. 5, for the initial condition

$$c_t(r, z, 0) = c_i(r, z) - c_f(r, z)$$

and the surface condition

$$-\rho k D \left(\frac{\partial c_t}{\partial r}\right)_{r=r_0} = P_m c_t(r_0, z, t), \quad -\infty < z < +\infty.$$

Then, as is readily shown, the function satisfying all conditions of the present problem is

$$c(r, z, t) = c_f(r, z) + c_t(r, z, t)$$

where $c_f(r, z)$ is given by Eq. 20a,b, in which c_0 is replaced by c_1.

After solving Eq. 5 for c_t by a method analogous to that given by Carslaw and Jaeger (1959, p. 211) the final result reads

$$\begin{aligned} c = c_f(r, z) - \frac{c_1 - c_0}{2}\Bigg(\sum_{n=1}^{\infty} \frac{J_0(\beta_n r/r_0)}{\beta_n(1 + \beta_n^2/L^2)J_1(\beta_n)} \\ \{\exp(\beta_n z\sqrt{k}/r_0)[\operatorname{erf}(\beta_n\sqrt{kDt}/r_0 + z/2\sqrt{Dt}) - 1] \\ + \exp(-\beta_n z\sqrt{k}/r_0)[1 - \operatorname{erf}(\beta_n\sqrt{kDt}/r_0 - z/2\sqrt{Dt})] \\ + 2\exp(-\beta_n^2 kDt/r_0^2)[1 - \operatorname{erf}(z/2\sqrt{Dt})]\}\Bigg). \end{aligned} \tag{29}$$

Also here, and by analogy with the treatment of the steady-state solutions it is of interest to provide the equation for the build up of the average concentration inside the bundle (see Eq. 18). Briefly, the way of writing this solution is to replace the function $J_0(\beta_n r/r_0)/J_1(\beta_n)$ in Eq. 29 by the factor $2/\beta_n$, the result being referred to as Eq. 30. It may finally be useful also to give the solution for the case where the surface layer of the bundle is absent, other conditions remaining unchanged: replace (*a*) the term $\beta_n(1 + \beta_n^2/L^2)$ in the denominator of Eq. 29 by α_n and (*b*) β_n in all functions by α_n. This solution will be referred to as Eq. 31.

The meaning of Eqs. 30 and 31 has been illustrated in two different ways: (*a*) in Fig. 4 by the plot of the concentration profiles along the bundle axis with (normalized) time as parameter and (*b*) in Fig. 5 by the time-course of the concentration change, the parameter here being the (normalized) distance along the bundle. A particular feature may be pointed out: first, it can be shown algebraically, but is also understood intuitively from symmetry considerations, that at $z = 0$ the time-course of concentration change (normalized as in Fig. 5) is identical to that obtained in every cross section of a cylindrical bundle subjected to a concentration step along its entire surface (i.e., over the distance $-\infty < z < +\infty$, cf. Eq. 47 in Hill [1928] and Eqs. [5.22] and [5.46] in Crank [1975]). Furthermore, it is evident that the concentration alters with the same time-course also at $z = -\infty$. However, in the intervening region ($-\infty < z < 0$), the time-course of concentration change is different, but this difference is only small. To illustrate this point, each curve at the extreme left in the panels of Fig. 5 was computed for the particular value of z, z_p, (in the range $z < 0$) where the largest deviation in

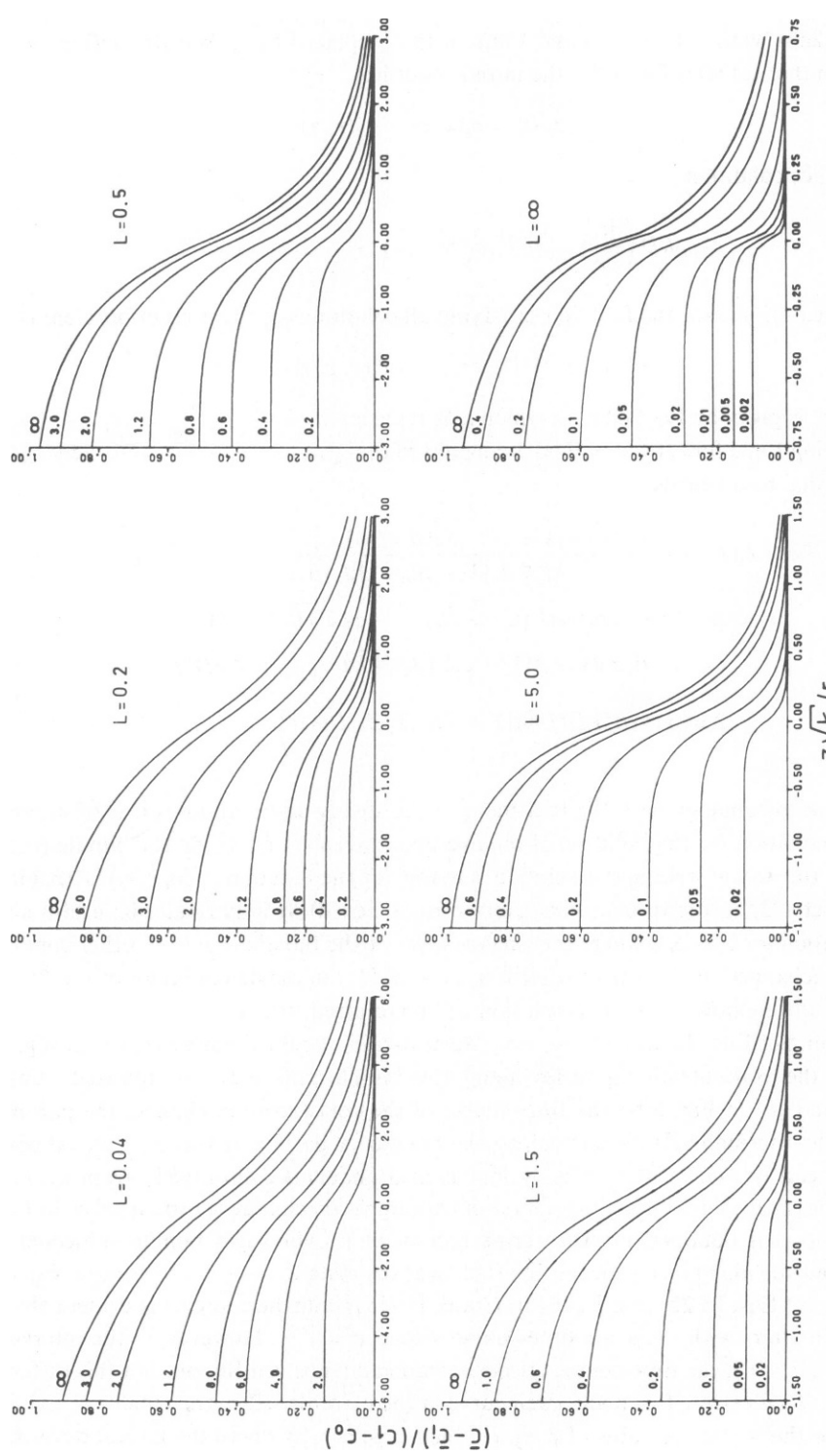

FIGURE 4 Concentration profiles in cylindrical bundle after step change of outside concentration from c_0 to c_1 in region $z < 0$; concentration in region $z > 0$ is kept constant $c = 0$; bundle position as in Fig. 1*A* with $-l \rightarrow -\infty$. Ordinate in terms of $(\bar{c} - \bar{c}_i)/(c_1 - c_0)$, where $\bar{c}_i$ initial, $\bar{c}$ concentration at time t, both average concentrations over cross section at point z. Numbers against curves, values of kDt/r_0^2. D diffusion coefficient; all other symbols as in Fig. 2.

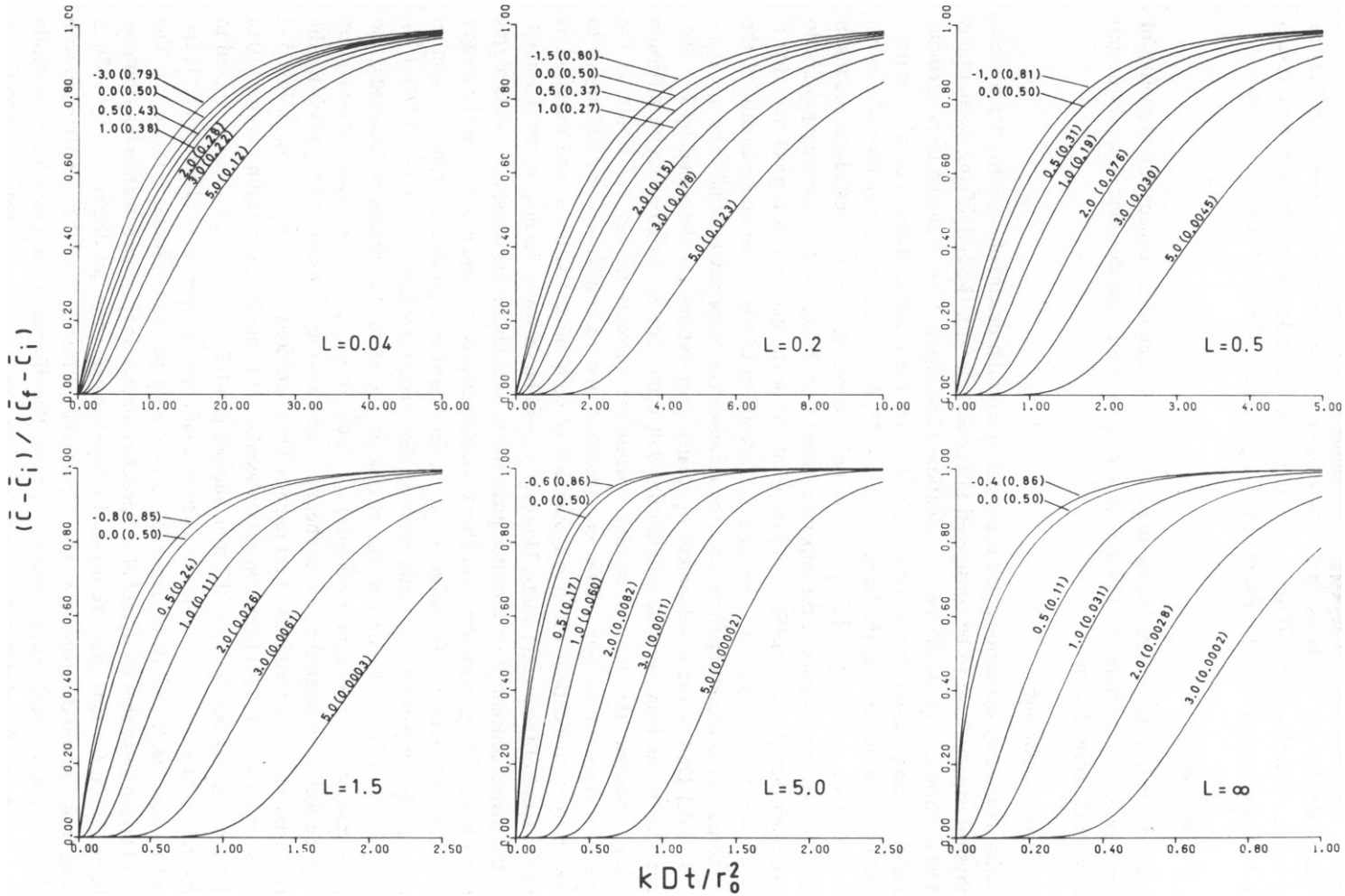

FIGURE 5 Time-course of concentration change at various points along bundle. $\bar{c}_f$ final (average) steady concentration in bundle at point z; numbers at curves, values of $zk^{1/2}/r_0$ or (in parentheses) of $(\bar{c}_f - \bar{c}_i)/(c_1 - c_0)$; cf. legend of Fig. 4.

time-course from that at $z = 0$ occurs. As the comparison of this curve with that immediately to its right (i.e., for $z = 0$) shows, in all cases concentration changes are more rapid in the region $-\infty < z < 0$ than at $z = 0$ (or $z = -\infty$), but the factor describing this increased rate is only ≤ 1.35, the largest value for the ratio $t_{1/2(z-0)}/t_{1/2(z-z_p)}$, of the half-times obtained.

DISCUSSION

The equations in this study were derived to permit calculations of the concentration profiles of saline and sucrose in the interstitial fluid spaces of heart muscle bundles placed in sucrose gap chambers of different designs.

Approximations

Before discussing the application of the equations to several problems of experimental interest, two physical aspects have to be considered in connection with the simplifying assumptions stated when formulating the differential equations of diffusion. First, it should be pointed out that steady concentration distributions derived from these assumptions, i.e., distributions computed by superposition on the basis of Eqs. 14, 23, or 26, satisfy the condition of osmotic equilibrium ($[Na^+] + [K^+] + [Cl^-] +$ [sucrose] = constant; osmotic coefficients are taken to be 1). This is a consequence of the important result that the steady concentration profiles do not depend on the diffusion coefficient of the solute. (For the mathematical proof note that if $c_T = c_{T,0} \cdot f(r, z)$ is the concentration of a salt according to one of the above equations, the sucrose concentration resulting from the same saline-sucrose interface is found to be $c_S = c_{S,0} \cdot [1 - f(r,z)]$.) During the development of steady distributions (as described by Eq. 29), however, deviations from osmotic equilibrium will occur due to different solute diffusion coefficients. Second, the assumption that membrane currents do not contribute to the concentration distributions needs closer consideration. Ion accumulation or depletion due to external current application, which is a function of both current strength and duration, is beyond the scope of the present study. However, as will be shown in the next paper (Lammel, 1981), the spatial concentration variation gives rise to local circuit currents; the results of this paper can be used to gain information about possible effects of these currents on the steady concentration distributions. To estimate such effects within a particular trabecula section ($z_1 \leq z \leq z_2$) a comparison was made between the current integral $I_j(z_1, z_2) = (1/F) \int_{z_1}^{z_2} i_j \, dz = (1/F) \int_{z_1}^{z_2} g_j(V_m - V_j) \, dz$ and the change in the axial flux driven by concentration gradients $\Delta M_{z,j}(z_1, z_2) = D_j \pi r_0^2 \rho [(\partial \bar{c}_j/\partial z)_{z-z_2} - (\partial \bar{c}_j/\partial z)_{z-z_1}]$, i.e., the total diffusion flux entering the section through the surface sheath. (j denotes the ion species; the symbols for the electric variables are defined in the next paper.) The conditions chosen were those of Fig. 5 *A* (curves 0) of Lammel (1981) (a frog atrial trabecula of 0.1-mm Diam extending from $z = 0$ to $z = 1.4$ mm; test section $0 < z < 0.2$ mm, sucrose gap $0.2 < z < 1$ mm, section exposed to isotonic KCl solution $1 < z < 1.4$ mm; current conducting properties of the cell membrane defined by Eqs. 9a, b and 10 of paper II; surface area per unit volume 7,400 cm^{-1}). The results obtained show that the effect of membrane currents on the concentration distributions can be neglected for ions that are driven by high concentration gradients, i.e., for sodium diffusing from the test compartment and for potassium diffusing from the compartment with isotonic KCl solution both into the sucrose section. The distribution of potassium ions within the test section and the adjoining sucrose region, however, must be expected to be modified to

some extent by the local circuit currents as indicated by the following computational results: $I_K(0, 0.1\text{ mm}) = -7.9 \cdot 10^{-15}$ mol s^{-1}, $\Delta M_{z,K}(0, 0.1\text{ mm}) = -1.6 \cdot 10^{-14}$ mol s^{-1}; $I_K(0.1, 0.2$ mm$) = 1.6 \cdot 10^{-14}$ mol s^{-1}, $\Delta M_{z,K}(0.1, 0.2\text{ mm}) = -7.3 \cdot 10^{-14}$ mol s^{-1}; $I_K(0.2, 0.3\text{ mm}) = 2.1 \cdot 10^{-14}$ mol s^{-1}, $\Delta M_{z,K}(0.2, 0.3\text{ mm}) = 7.1 \cdot 10^{-14}$ mol s^{-1}; $I_K(0.3, 0.4\text{ mm}) = 4.6 \cdot 10^{-15}$ mol s^{-1}, $\Delta M_{z,K}(0.3, 0.4\text{ mm}) = 1.5 \cdot 10^{-14}$ mol s^{-1}. (The negative sign of I_K defines inward direction of potassium current; the negative sign of $\Delta M_{z,K}$ inward direction of diffusion flux through the surface sheath.) Thus, except at the end of the test section ($0 < z < 0.1$ mm) where both $\Delta M_{z,K}$ and I_K are so small that they produce only slight deviation of the interstitial concentration from that of the bathing fluid (cf. concentration profiles of Fig. 6 below), the membrane current may represent a potassium flux that is maximally ~30% of the diffusional flux.

Parameter Values

To use the equations it is necessary to know the numerical value of the parameter L appropriate for each preparation concerned. At this point, the main problem is that of obtaining sufficiently accurate estimates for P_m, since the two other parameters contained in the definition of L(Eq. 17), r_0 and ρ, are readily obtained through histological and other methods. The position is relatively straightforward in the case of frog ventricular trabeculae for which both the approximate size and number of pathways across the endothelial cell layer of the trabeculae are known. Thus, on the basis of the electron-microscope data provided by Page and Niedergerke (1972; Table 2 and their Eq. 2) P_m can be calculated and comes to $3.9 \cdot 10^{-5}$ cm s^{-1}, when the diffusion coefficient $D = 8 \cdot 10^{-6}$ cm^2 s^{-1}. (For convenience, this value for D, that of calcium ion, is used throughout this section, but since P_m is proportional to D figures obtained for P_m are readily converted to those appropriate for any other solute.) For a trabecula of radius $r_0 = 0.05$ mm and $\rho = 0.1$ (Page and Niedergerke, 1972) the value for L comes to 0.3 (independent of D, cf. page 539).

In all other preparations commonly used for voltage-clamp experiments, i.e., frog atrial and mammalian heart trabeculae, histological data of this kind are missing and indirect procedures have to be found to obtain P_m and L. (In any case, methods of this kind should be applied in addition to calculations from morphometric data.)

The procedure used for frog atrial trabeculae is based on the experimental finding (Chapman and Niedergerke, 1970) that an initial, rapid twitch response to a step change of external calcium concentration is controlled by the rate with which the new level of calcium concentration is established at cell surfaces of the constituent fibers within the bundle. When the experimental conditions are chosen to be such (e.g. Niedergerke and Page, 1977; Fig. 3) that the strength of the heart-beat rises in direct proportion to the external calcium concentration, then the time-course of this response should follow a curve of the kind plotted for $z = 0$ in Fig. 5. The experimental half time ($t_{1/2}$) of the response concerned was found to be ~2.7 s (Lammel et al., 1975) and this, together with appropriate figures for r_0(0.05 mm), ρ(0.27) and D (as above), gives a value of 0.72 for the term $kDt_{1/2}r_0^{-2}$ (for definition of k, see Eq. 10). When this parameter is entered into the appropriate panel of Fig. 5 (panel 3) half-saturation of diffusion is shown to occur with a value of L close to 0.5, yielding $P_m = 1.8 \cdot 10^{-4}$ cm s^{-1}. It should be mentioned that there is greater permeability of the endothelium cell layer in frog atrium compared with that in ventricle, expressed by the ratio of

the coefficients $P_{m(atrium)}/P_{m(ventricle)} = 4.6$, because the pathways through this layer are both shorter and wider in atrial than ventricular preparations, as was shown by an electron-microscope comparison (Lammel et al., 1975). In the case of mammalian trabeculae, P_m was estimated from the electrical resistance, R_m, of the endothelium cell layer by the relation $P_m = D/(R_m \cdot \sigma)$, where σ is the conductivity of Ringer's fluid: $0.0125\Omega^{-1}\,cm^{-1}$. First, current and potential data from Beeler and Reuter (1970) were converted by the procedure suggested by Attwell and Cohen (1977) to obtain a value of 400 Ω for the resistance of the endothelial sheath surrounding the bundle segment in the test compartment. Referring this to unit area for the preparation concerned (diameter of trabecula: 0.5 mm, length: 1 mm) one obtains $P_m = 1 \cdot 10^{-4}\,cm\,s^{-1}$ and $L \sim 1.5$.

Conclusions

Figs. 6–8 provide examples illustrating the application of the equations derived to particular experimental conditions. Fig. 6 shows the diffusion profiles along frog atrial trabeculae in sucrose gap arrangements that contain either a single (6 *A* and *B*) or double (*C*) gap, where the dimensions of test and sucrose segments, of 200 and 400 μm, respectively, were chosen to approximate the situation of the experiments of Rougier et al. (1968). The curves for sodium and potassium concentration were calculated by Eq. 19 a, b, using the superposition principle to allow for the contribution of ion fluxes from several different saline-sucrose junctions (two junctions in the case of the single gap, four junctions in the case of the double gap). In the test segment of the single-gap arrangement (Fig. 6 *A* and *B*) the sodium concentration is seen to rise from a 50 to 100% level between saline-sucrose junction and the (left) end of the model. The average over the whole of this segment amounts to 85%; all concentrations are expressed as percentage of that in Ringer's fluid. Concentrations in the double sucrose gap arrangement come to 82 and 72% for the maximum and average, respectively: clearly less favorable than for the single gap. Of course, these concentration levels depend critically on the dimensions chosen for both preparation and experimental chamber. For example, the maximal and average concentrations should be substantially lower in the double sucrose gap arrangement used by Tarr and Trank (1974) who gave a test segment of 100-μm length and a preparation diameter of 300–500 μm. Taking these figures (a bundle diameter of 400 μm) one obtains levels of only 32 and 24%, for the maximum and average, respectively. However, these values cannot be accepted without reservation because, quite frequently, trabeculae of large diameter are composed of (at least partly) separate, smaller bundles whose diameter would have to be known for more precise calculations (Lammel et al., unpublished data).

The concentration profiles of Fig. 7 illustrate several features of a (single) sucrose gap arrangement, on the basis of only one saline-sucrose junction; the other junction (sucrose-saline) is taken to be so far away that its effects are negligible. The dimensions chosen are appropriate for a mammalian trabecula (Reuter and Scholz, 1977), preparation diameter: 0.5 mm, length of test segment: 0.6 mm; $L = 1.5$, cf. above). Three points were examined: (*a*) of curves 3 and 4 (Fig. 7 *A*), curve 4 was calculated by Eq. 19a, b, curve 3 by Eq. 23a, b. Thus, radial diffusion within the interstitial fluid spaces was either included or neglected (note, in neither case was a partition present). That this radial diffusion process contributes little to the setting up of the concentration profiles is indicated by the similar shape and position of the two curves. This important point is discussed in greater detail below. (*b*) Comparison of curves 1

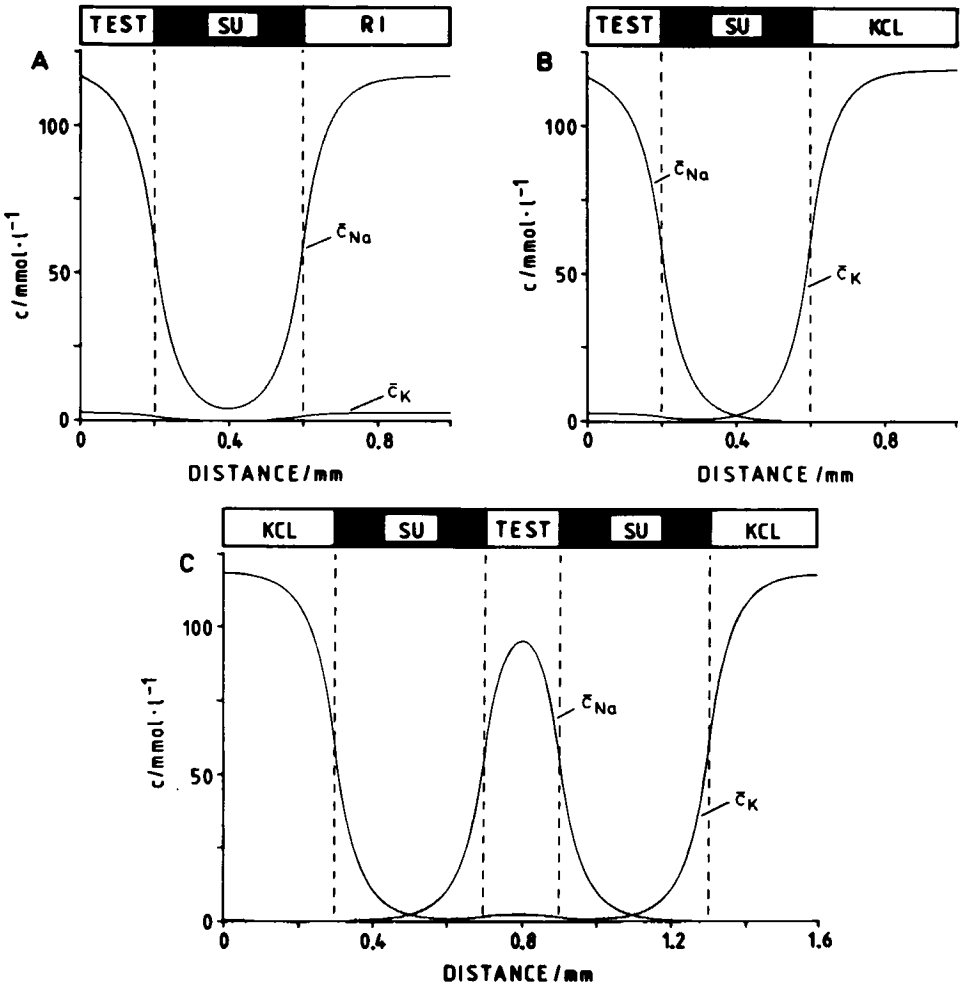

FIGURE 6 Longitudinal distribution of average cross-sectional concentration of sodium ($\bar{c}_{Na}$) and potassium ($\bar{c}_K$) in a frog atrial trabecula (0.1-mm Diam). *A* and *B*, single sucrose gap arrangement: length of test, sucrose and reference segments: 0.2, 0.4, and 0.4 mm respectively; *C*, double sucrose gap with test segment of 0.2 mm, two sucrose segments of 0.4 mm each and reference segments of 0.3 mm length. Solutions in different compartments: TEST and RI, Ringer solution c_{Na} = 116.5 mmol/liter, c_K = 2.5 mmol/liter; KCL, isotonic KCl solution c_K = 119 mmol/liter; SU, isotonic sucrose solution.

or 2 with curve 3 (Fig. 7 *A*) illustrates the effects expected to arise when a partition is present at the fluid junction. Two different widths of the partition were assumed for the computation of profiles 1 and 2 (0.1 and 0.2 mm, respectively) as indicated by the vertical lines. As is clear from inspection of the three curves, a partition enhances the ion concentration in the whole test segment but at the cost of extending the region of high concentration into the remaining part of the bundle, especially into the region inside the partition. (*c*) In Fig. 7 *B* a partition 0.1-mm wide was used to demonstrate the effects of tissue compression by this partition. In both cases illustrated (curves 5 and 6, calculated by Eq. 26) the compressed cross-sectional area was 60% of the original size. In one case (curve 5) ρ, the fractional interstitial space,

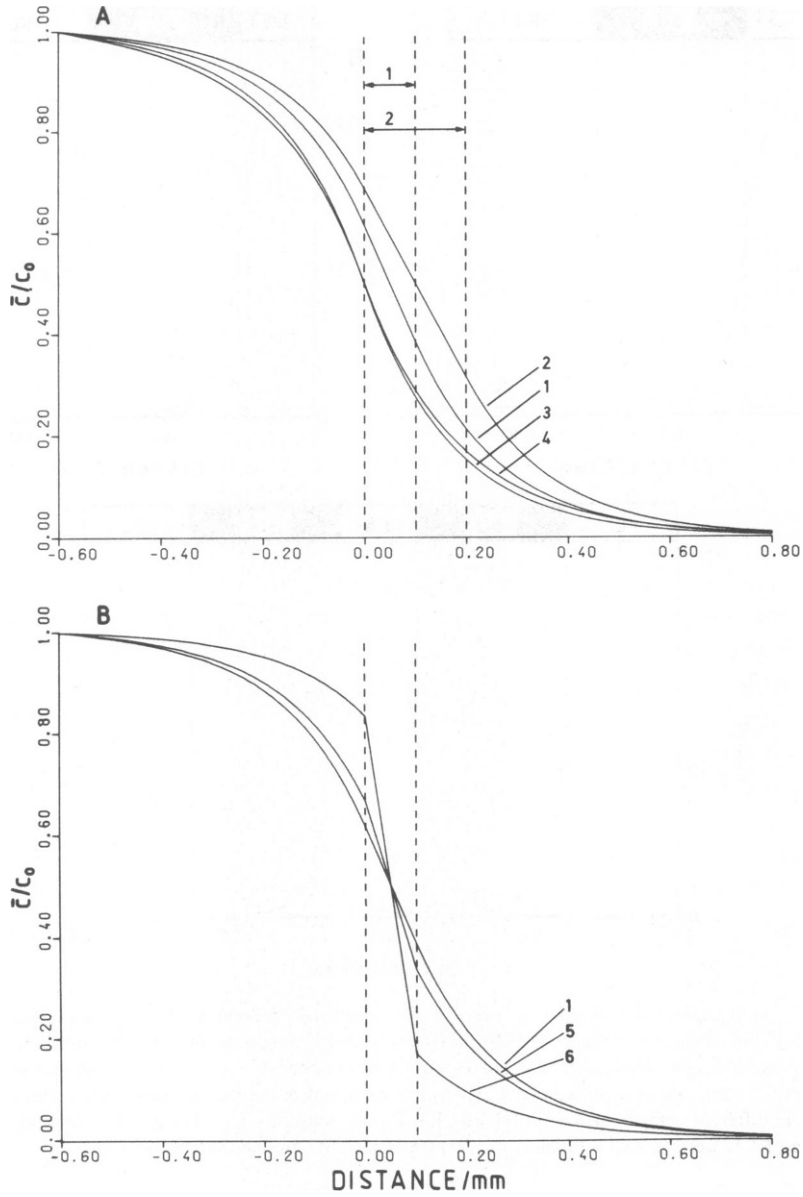

FIGURE 7 Average concentration of saline along mammalian ventricular bundle (0.5-mm Diam). *A*, curves 1 and 2: partition either of 0.1 mm (1) or 0.2 mm (2) width present indicated by dashed lines; curves 3 and 4: no partition, radial diffusion neglected for curve 3. *B*, curve 1 as curve 1A; curves 5 and 6: compression of bundle by partition in each case to 60% of original cross-section; curve 5, $H = 1/0.6$; curve 6, $H = 1/0.15$, cf. Eq. 27 and text.

remained constant; in the other (curve 6) it was diminished to a quarter of its original value: i.e., the proportion of fluid squeezed from the interstitial and cellular volume was either the same (curve 5) or else the proportion squeezed from the interstitial volume was much greater than that from the cellular volume (curve 6). As was expected, the condition of reduced ρ

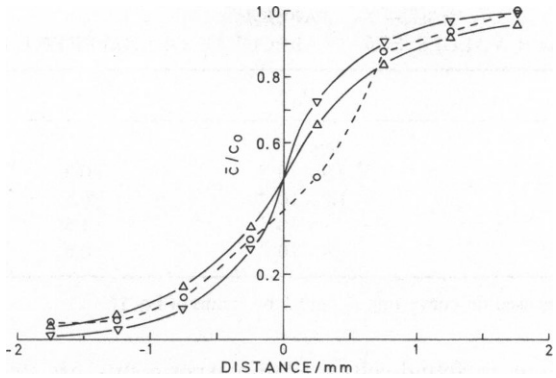

FIGURE 8 Longitudinal distribution at both sides of a saline-sucrose junction of sodium in mammalian ventricular trabeculae from experiments of Kléber (1973). Experimental values (O), those calculated by means of Eq. 21a,b (∇) for bundles of 1-mm or (Δ) 2-mm Diam. Permeability coefficient of surface sheath $P_m = 4.10^{-5}$ cm s^{-1}; $k = 0.83$ (see text). Saline-sucrose junction at zero of abscissa with sucrose on the left. Kléber's results rescaled.

produces the more striking effect: the salt concentration in the test segment is much enhanced and the concentration gradient under the partition is steepened. This result alone would favor more precise current recording than is otherwise possible (see subsequent papers). Whether it can be achieved without causing extensive tissue injury appears to be worth examining.

In Fig. 8 the present model is applied to the results of Kléber (1973) who studied the steady diffusion profiles of radioactive sodium ions at both sides of a saline-sucrose partition, in sheep and calf ventricular trabeculae, 1–2 mm thick. As is shown, the two curves, constructed with Eqs. 21a, b and drawn through the two sets of triangles, provide a good fit to Kléber's data (circles), with $P_m = 4 \cdot 10^{-5}$ cm s^{-1}. (For an earlier attempt to fit Kléber's data on the basis of a less complete model, see Attwell and Cohen, 1977; Fig. 8). Different experimental approaches that would seem feasible for testing the predictions of the model are for example the use of ion-selective microelectrodes (cf. Kline and Morad, 1978) or of fluorescent dyes. The latter method has already been applied by Salama and Morad (1977) to determine the extracellular solute distribution in a sucrose gap arrangement. The space constant (Λ) of 190 μm obtained by these authors for frog ventricle strips of 0.5–1-mm Diam agrees well with the value calculated with Eq. 22 ($r_0 = 0.35$ mm, $P_m = 3.9 \cdot 10^{-5}$ cm s^{-1}, $\rho = 0.1$: $\Lambda = 189$ μm). However, because frog preparations of such large diameter are most frequently composed of several smaller bundles, a direct comparison of these two values may be inadequate.

Table I summarizes values for both P_m and L as determined or used above. The main result is that L extends over a range of fairly low values, from 0.3 to 1.5; the significance of this becomes clear in Fig. 2. Thus, for $0.5 < L < 1.5$ radial concentration gradients in the interstitial fluid spaces are only small over much of the bundle length. This, indeed, provides the explanation for the lack of any major difference between curves 3 and 4 of Fig. 7 *A*, and it also suggests the following conclusion: when setting up models to examine the potential and current changes occurring in voltage-clamp experiments with these preparations, it is possible, to a first approximation, to neglect effects due to radial variation of ionic concentrations in the external medium. This simplifies the mathematics considerably.

The final point to be discussed concerns the kinetics of the diffusion process. The question

TABLE I
PARAMETER VALUES FOR TRABECULAE OF DIFFERENT HEARTS

Preparation	P_m	L	r_0*
	($cm\ s^{-1}$)		(mm)
Frog ventricle	$3.9 \cdot 10^{-5}$	0.3	0.05
Frog atrium	$1.8 \cdot 10^{-4}$	0.5	0.05
Dog ventricle	$1 \cdot 10^{-4}$	1.5	0.25
Sheep, calf ventricle	$4 \cdot 10^{-5}$	0.5	0.25

*r_0: bundle radius, which was used for converting P_m into L by means of Eq. 16.

was asked: to what extent, in actual voltage-clamp experiments, are steady diffusion profiles established by the time potential and current recording commences, once sucrose is introduced into the gap. (This question was recently raised by Beeler and McGuigan, 1978.) Again, the dimensions chosen were those of a mammalian trabecula (r_0 = 0.25 mm, L = 1.5), and the times were calculated for concentration changes of NaCl in the center of (*a*) test and (*b*) sucrose segment to attain either 50 or 90% completion (the arrangement being a single saline-sucrose junction as in Fig. 7 *A*). These periods of time as obtained by Eq. 30 (Fig. 5), come to 15 and 35 s for the 50% concentration level and to 55 and 80 s for the 90% level, in the sucrose and test segment, respectively. Thus, the establishment of the profiles is fairly rapid and even for trabeculae of low surface permeability (r_0 = 0.25 mm, L = 0.5) occurs within $<\sim$5 min. It should be noted, however, that these time periods are likely to be underestimated since the presence of narrow spaces and clefts between cells (cf. page 534), which tend to slow down the diffusion process, has been ignored.

I am indebted to Dr. R. Niedergerke, Dept. of Biophysics, University College London, for suggesting the problem and for his help and encouragement throughout this work.

Received for publication 26 August 1980 and in revised form 8 April 1981.

REFERENCES

Adrian, R. H., W. K. Chandler, and A. L. Hodgkin. 1969. The kinetics of mechanical activation in frog muscle. *J. Physiol. (Lond.)* 204:207–230.

Anderson, N. C. 1969. Voltage-clamp studies on uterine smooth muscle. *J. Gen. Physiol.* 54:145–165.

Attwell, D., and I. Cohen. 1977. The voltage clamp of multicellular preparations. *Prog. Biophys. Mol. Biol.* 31:201–245.

Beeler, G. W., and J. A. S. McGuigan. 1978. Voltage clamping of multicellular myocardial preparations: capabilities and limitations of existing methods. *Prog. Biophys. Mol. Biol.* 34:219–254.

Beeler, G. W., and H. Reuter. 1970. Voltage clamp experiments on ventricular myocardial fibres. *J. Physiol. (Lond.)* 207:165–190.

Berger, W. 1963. Die Doppelsaccharosetrennwandtechnik: eine Methode zur Untersuchung des Membranpotentials und der Membraneigenschaften glatter Muskelzellen. *Pflügers Archiv. Gesamte Physiol. Menschen Tiere.* 277:570–576.

Brown, H. F., and S. J. Noble. 1969. Membrane currents underlying delayed rectification and pace-maker activity in frog atrial muscle. *J. Physiol. (Lond.)* 204:717-736.

Bülbring, E., and M. F. Shuba (editors). 1976. Physiology of Smooth Muscle. Raven Press, New York.

Carslaw, H. S., and J. C. Jaeger. 1959. Conduction of Heat in Solids. Clarendon Press, Oxford, England.

Chapman, R. A., and R. Niedergerke. 1970. Effects of calcium on the contraction of the hypodynamic frog heart. *J. Physiol. (Lond.)* 211:389–421.

Crank, J. 1975. The mathematics of Diffusion. Clarendon Press, Oxford, England.

Goldman, Y., and M. Morad. 1977. Measurement of transmembrane potential and current in cardiac muscle: a new voltage clamp method. *J. Physiol. (Lond.)* 268:613–654.

Haas, H. G., R. Kern, and H. M. Einwächter. 1970. Electrical activity and metabolism in cardiac tissue: an experimental and theoretical study. *J. Membr. Biol.* 3:180–209.

Harrington, L., and E. A. Johnson. 1973. Voltage clamp of cardiac muscle in a double sucrose gap. A feasibility study. *Biophys. J.* 13:626–647.

de Hemptinne, A. 1976. Voltage clamp analysis in isolated cardiac fibres as performed with two different perfusion chambers for double sucrose gap. *Pfluegers Arch. Eur. J. Physiol.* 363:87–95.

Hill, A. V. 1928. The diffusion of oxygen and lactic acid through tissues. *Proc. R. Soc. Lond.* B104:39–96.

Johnson, E. A., and M. Lieberman. 1971. Heart: excitation and contraction. *Annu. Rev. Physiol.* 33:479–532.

Kantorovich, L. V., and V. T. Krylov. 1958. Approximate Methods of Higher Analysis. Interscience-Noordhoff, Groningen, Holland.

Kléber, A. G. 1973. Effects of sucrose solution on the longitudinal tissue resistivity of trabecular muscle from mammalian heart. *Pfluegers Arch. Eur. J. Physiol.* 345:195–205.

Kline, R. P., and M. Morad. 1978. Potassium efflux in heart muscle during activity: extracellular accumulation and its implications. *J. Physiol. (Lond.).* 280:537–558.

Kootsey, J. M., and E. A. Johnson. 1972. Voltage clamp of cardiac muscle. A theoretical analysis of early currents in the single sucrose gap. *Biophys. J.* 12:1496–1508.

Lammel, E. 1981. A theoretical study on the sucrose gap technique as applied to multicellular muscle preparations: II. Methodical errors in the determination of outward currents. *Biophys. J.* 36:555–573.

Lammel, E., R. Niedergerke, and S. Page. 1975. Analysis of a rapid twich facilitation in the frog heart. *Proc. R. Soc. Lond.* B189:577–590.

Mathias, R. T., R. S. Eisenberg, and R. Valdiosera. 1977. Electrical properties of frog skeletal muscle fibres interpreted with a mesh model of the tubular system. *Biophys. J.* 17:57–93.

McGuigan, J. A. S. 1974. Some limitations of the double sucrose gap, and its use in a study of the slow outward current in mammalian ventricular muscle. *J. Physiol. (Lond.)* 240:775–806.

McLennan, H. 1956. The diffusion of potassium, inulin, and thiocyanate in the extracellular spaces of mammalian muscle. *Biochim. Biophys. Acta.* 21:472–481.

Morad, M., and Y. Goldman. 1973. Excitation-contraction coupling in heart muscle: membrane control of development of tension. *Prog. Biophys. Mol. Biol.* 27:257–313

Morad, M., and R. K. Orkand. 1971. Excitation-concentration coupling in frog ventricle: Evidence from voltage clamp studies. *J. Physiol. (Lond.)* 219:167–189.

New, W., and W. Trautwein. 1972. Inward membrane currents in mammalian myocardium. *Pflügers Arch. Eur. J. Physiol.* 334:1–23.

Niedergerke, R., and S. Page. 1977. Analysis of catecholamine effects in single atrial trabeculae of the frog heart. *Proc. R. Soc. Lond.* B197:333–362.

Page, S. G., and R. Niedergerke. 1972. Structures of physiological interest in the frog heart ventricle. *J. Cell Sci.* 11:179–203.

Poindessault, J. P., A. Duval, and C. Léoty. 1976. Voltage clamp with double sucrose gap technique. External series resistance compensation. *Biophys. J.* 16:105–120.

Ramón, F., N. Anderson, R. W. Joyner, and J. W. Moore. 1975. Axon voltage-clamp simulations. IV. A multicellular preparation. *Biophys. J.* 15:55–69.

Reuter, H., and H. Scholz. 1977. A study of the ion selectivity and the kinetic properties of the calcium dependent slow inward current in mammalian cardiac muscle. *J. Physiol. (Lond.)* 264:17–47

Rougier, O., G. Vassort, and R. Stämpfli. 1968. Voltage clamp experiments on frog atrial heart muscle fibres with the sucrose gap technique. *Pflügers Archiv Gesamte Physiol. Menschen Tiere.* 301:91–108.

Salama, G., and M. Morad. 1977. Use of fluorescent dyes to evaluate single sucrose gap voltage clamp technique in frog heart. *Biophys. J. (Abstr.).* 17:5*a*.

Schneider, M. F. 1970. Linear electrical properties of the transverse tubules and surface membrane of skeletal muscle fibers. *J. Gen. Physiol.* 56:640–671.

Sommer, J. R., E. A. Johnson. 1979. Ultrastructure of cardiac muscle. *In* Handbook of Physiology. (Sect. 2) Vol. I. 113–186.

Tarr, M., and J. Trank. 1971. Equivalent circuit of frog atrial tissue as determined by voltage clamp–unclamp experiments. *J. Gen. Physiol.* 58:511–522.

Tarr, M., and J. W. Trank. 1974. An assessment of the double sucrose-gap voltage clamp technique as applied to frog atrial muscle. *Biophys. J.* 14:627–643.

Trautwein, W. 1973. Membrane currents in cardiac muscle fibers. *Physiol. Rev.* 53:793–835.